ELECTRON SCATTERING FROM A TENSOR POLARIZED ^{2}H INTERNAL TARGET *)

J.F.J. VAN DEN BRAND

NIKHEF, Amsterdam, The Netherlands

and

Department of Physics, University of Wisconsin-Madison, Madison, Wisconsin 53706, USA

Received 24 January 1995

An experiment (NIKHEF 91-12) is described which measures the spin dependence of the (e,e) and (e,e'p) reactions for polarized deuterium and unpolarized electrons, using the Internal Target Hall facility at the Amsterdam Pulse Stretcher Ring at NIKHEF. Tensor polarized deuterium is produced in an atomic beam source and injected into a storage cell target. Polarimeters are used to monitor the target polarization. A large acceptance non-magnetic detector system is used for the electron-proton (deuteron) coincidence measurement. It is demonstrated that these techniques result in low backgrounds due to scattering from species other than the polarized target gas and allow for fast and flexible orientation of the target spin. Specific issues such as interfacing the experiment to the storage ring and monitoring the performance of the target system are discussed in detail.

Contents

*) Lectures given at the Indian-Summer school on Electron Scattering of Nucleons and Nuclei, Prague (Czech Republic), September 1994.

1 Introduction

The use of a polarized gas target internal to an electron storage ring has many advantages in the measurement of spin-dependent electromagnetic scattering observables [1]. Several efforts are planned or under way at laboratories worldwide to undertake measurements using this technique [2–5]. We report here the technical details of measurements carried out using the Amsterdam Pulse Stretcher ring, AmPS, with a tensor polarized ^{2}H target and an electron beam.

The experiment was designed to employ polarization observables for an enhanced investigation of the dynamical features of the deuteron. In addition to the spin structure of the ^{2}H ground state, the polarized ^{2}H nucleus has the added feature that it is a good approximation to a polarized neutron. Thus, it should be possible to determine the charge [6] and spin [7] distributions of the neutron from measurement of quasi-elastic and deep inelastic electron scattering from polarized ^{2}H. The charge distribution of the neutron has long been identified as a fundamental measurement and a number of experiments using polarized ^{2}H are planned [8] at intermediate energy electron facilities. Recently, the first deep inelastic measurements of spin-dependent scattering from polarized ^{2}H have been carried out and further experiments are planned at SLAC and DESY.

Crucial to the extraction of precise information on the neutron is an understanding of the spin structure of the ^{2}H ground-state wave function. This is best determined using medium energy quasi-elastic spin-dependent electron scattering from polarized ^{2}H. In addition, it is important to obtain a quantitative understanding of the corrections to the simple impulse approximation of the quasi-elastic reaction mechanism, e.g. final-state interactions, in the kinematic regimes used.

The experiment made use of the novel technique of a polarized internal target with an electron beam in a storage ring. In Section 2 an overview of the physics of the experiment is given. Section 3 discusses some overall aspects of the experiment. In Section 4 the operation of the polarized ^{2}H internal gas target is described. A description of the performance of the apparatus is discussed in Section 5.

2 Physics

The ultimate goal of nuclear physics is to give a complete description of the structure of the atomic nucleus, a dense quantum system of fermions with a relatively small number of interacting constituents. The starting point is the detailed nucleon-nucleon (NN) interaction which is extremely complicated and deduced from NN scattering data and the properties of the deuteron. After fitting the parameters to the data one employs three-nucleon observables for fixing the off-shell behavior. Once the correct two-nucleon potential is determined one then calculates the structure of heavier nuclei for example using the independent-pair model.

In the last three decades an extensive intellectual activity has taken place alone these lines using a non-relativistic, nucleons-only approach. However, at present there is still no consensus on which NN interaction is most accurate. Furthermore, it is unknown whether the formalism with only pair-wise interactions is adequate.

One of the corner-stones are the bound-state properties of the deuteron and all realistic NN potentials are in good agreement with the available data. The magnetic moment of the deuteron, $\mu_d = 0.87925$ nm, is in good approximation given by the sum of the proton and neutron magnetic moments, $\mu_p + \mu_n = 2.79275 - 1.91350 = 0.85735$ nm. Therefore, the deuteron ground-state wave function is predominantly S-wave. However, the non-zero quadrupole moment clearly implies the presence of a D-wave admixture induced by the tensor force and it is the prediction for this D-state probability which is the most significant difference between the various realistic NN potentials. P_D is a small quantity, probably between 2 and 7 %. Measurement of electromagnetic spin observables is known for its precision in extracting small amplitudes of considerable importance for understanding the dynamics of nucleons and few-body systems.

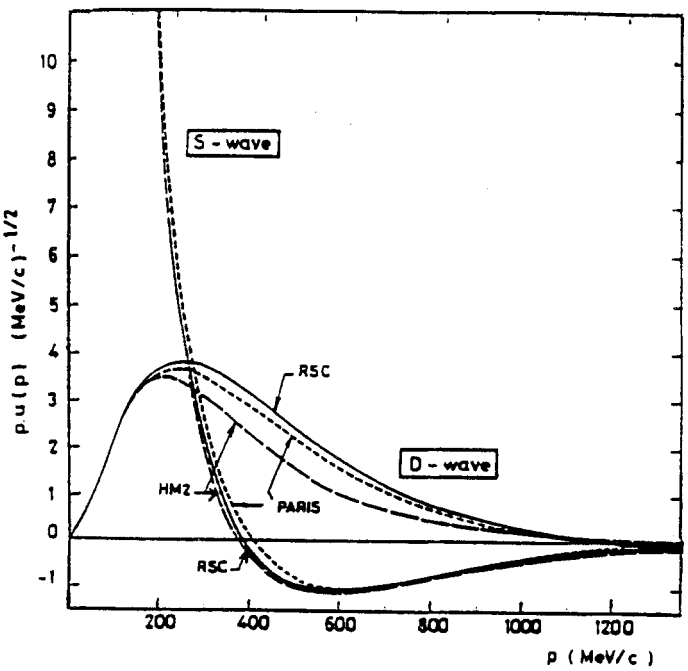

Fig. 1. The S-wave and the D-wave functions of the deuteron ground state in momentum space for various NN potentials. HM2 is a variation of the Bonn NN potential.

In an attempt to address this question, experiment 91-12 will study the spin structure of deuterium using spin-dependent electron scattering. The deuteron wave function can be written as:

$$\psi^{\sigma_d}(\vec{r}) = \sum_{L=0,2} \frac{1}{r} u_L(r)[\mathcal{Y}_L(\vec{r}) \times \chi_1(\mathrm{n,p})]_1^{\sigma_d} \qquad (1)$$

with $\vec{r} = \vec{r}_n - \vec{r}_p$. The conjugate variable is $\vec{p} = \frac{1}{2}(\vec{p}_n - \vec{p}_p)$ and in momentum space

the wave function can be written as:

$$\psi^{\sigma_d}(\vec{p}) = \sum_{L=0,2} u_L(p)[\mathcal{Y}_L(\vec{p}) \times \chi_1(\mathrm{n,p})]_1^{\sigma_d} \tag{2}$$

where the S- and D-wave functions

$$u(p) = \sqrt{\frac{2}{\pi}} \int j_0(pr) u_0(r) r \mathrm{d}r, \quad \text{and} \quad w(p) = -\sqrt{\frac{2}{\pi}} \int j_2(pr) u_2(r) r \mathrm{d}r \tag{3}$$

($u = u_0$, $w = u_2$) are shown for various realistic NN potentials in Fig. 1.

Using electron scattering off polarized deuterium there are two ways to obtain information on the S/D ratio:

- In elastic electron scattering the cross section is dominated by the form factor $A(q^2)$, $\mathrm{d}\sigma/\mathrm{d}\Omega \propto A(q^2)$. The A form factor is the sum of an S-wave and a D-wave contribution which can only be separated using spin observables.
- In quasi-elastic electron scattering the electron-proton coincidence cross section is proportional to the proton momentum distribution, $\mathrm{d}^6\sigma \propto \rho(p)$. Also $\rho(p)$ contains an S-wave and D-wave contribution.

Next we discuss how the relevant information on the S and D-wave function components is contained in these observables. We start with a discussion of the new results in elastic electron-deuteron scattering where for the first time the charge monopole and quadrupole electric form factors of the deuteron were separated.

2.1 Spin-dependent elastic electron scattering

For elastic deuteron scattering we have $I_\mathrm{i} = 1$, $I_\mathrm{f} = 1$ and consequently three form factors: the charge monopole G_C, quadrupole G_Q and the magnetic dipole G_M. At forward scattering angles the magnetic dipole contribution can be neglected. The monopole and quadrupole form factors can be written as

$$G_\mathrm{C} = G_\mathrm{ES} \int \{u^2(r) + w^2(r)\} j_0\left(\tfrac{1}{2}qr\right) \mathrm{d}r\,, \tag{4}$$

$$G_\mathrm{Q} = G_\mathrm{ES} \frac{3}{\eta\sqrt{2}} \int w(r) \left\{ u(r) - \frac{w(r)}{\sqrt{8}} \right\} j_2\left(\tfrac{1}{2}qr\right) \mathrm{d}r\,, \tag{5}$$

where G_ES and G_MS are the isoscalar electric and magnetic form factors of the nucleon, $j_0(\frac{1}{2}qr)$ and $j_2(\frac{1}{2}qr)$ are spherical Bessel functions, $\eta = q^2/4M_\mathrm{d}^2$ and $q^2 = \vec{q}^2 > 0$.

The unpolarized electron-deuteron elastic scattering cross section has been parameterized as follows

$$\frac{\mathrm{d}\sigma}{\mathrm{d}\Omega} = \sigma_\mathrm{Mott} \left[A(q^2) + B(q^2) \tan^2\left(\tfrac{1}{2}\theta_\mathrm{e}\right)\right]. \tag{6}$$

The form factors $A(q^2)$ and $B(q^2)$ are given by

$$A(q^2) = G_C^2(q^2) + \frac{8}{9}\eta^2 G_Q^2(q^2) + \frac{2}{3}\eta G_M^2(q^2)\,,\ B(q^2) = \frac{4}{3}\eta(1+\eta)G_M^2(q^2) \qquad (7)$$

and can be separated using the Rosenbluth technique. A complete separation of all three multipole form factors requires polarization observables.

With tensor-polarized deuterium the elastic electron scattering cross section can be written as

$$\frac{d\sigma}{d\Omega} = \frac{d\sigma_0}{d\Omega}[1 + T_{20}t_{20} + 2T_{21}\mathrm{Re}\,t_{21} + 2T_{22}\mathrm{Re}\,t_{22}]\,, \qquad (8)$$

where T_{20}, T_{21} and T_{22} are the components of the tensor analyzing power in a spherical basis, and t_{20}, t_{21} and t_{22} are the corresponding tensor-polarization parameters of the target. T_{20} may be expressed in terms of the deuteron form factors:

$$T_{20} = -\sqrt{2}\frac{[X(X+2) + \frac{1}{2}Y]}{[1 + 2(X^2 + Y)]}\,, \qquad (9)$$

in which $X = \frac{2}{3}\eta(G_Q/G_C)$, $Y = \frac{1}{3}\eta(G_M/G_C)^2 f(\theta)$, $f(\theta) = [1 + 2(1+\eta)\tan^2(\frac{1}{2}\theta)]$. The expression for t_{20} is

$$t_{20} = \frac{p_{zz}}{\sqrt{2}}P_2(\vec{n}\cdot\vec{q}), \qquad (10)$$

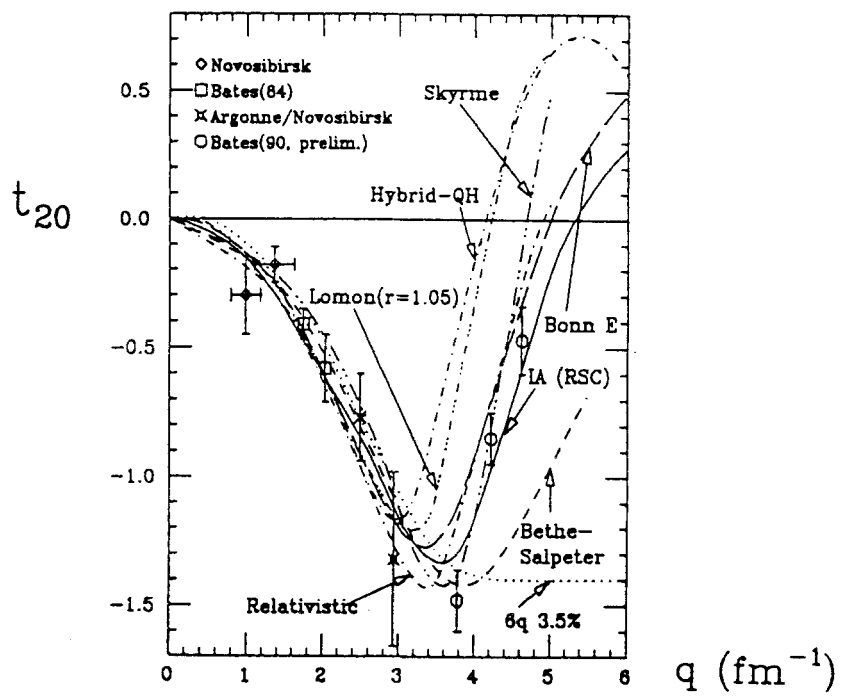

Fig. 2. Observable t_{20} for elastic electron-deuteron scattering. The curves are predictions from different models and are explained in Ref. 9.

where $p_{zz} = 1 - 3n_0$ is the Cartesian tensor polarization, n_0 is the fraction of deuterium atoms with a spin projection of zero, P_2 is the second Legendre polynomial, and $\vec{q}$ and $\vec{n}$ are unit vectors in the direction of $\vec{q}$ and the target polarization, respectively.

Recently, tensor polarization in elastic scattering has been measured both at VEPP-3 using a polarized internal target and at MIT-Bates using a deuteron polarimeter. The results for t_{20} are shown in Fig. 2.

The spin-dependent data have been used together with the Rosenbluth data to obtain the deuteron monopole form factor and a node has been observed at $q = 4.45 \pm 0.15$ fm^{-1} which is sensitive to the short-range repulsion of the NN interaction. It is remarkable that the non-relativistic IA [9] without MEC contributions is in good agreement with the data. The same model requires MEC contributions to give good agreement for the form factors of three- and four-body nuclei.

2.2 ^{2}H(e,e'p) quasi-elastic scattering

Electrodisintegration of the deuteron has been proven to be an essential tool for the study of the structure of the two-nucleon system. Coincidence ^{2}H(e,e'p) experiments under conditions of quasi-free kinematics have provided the most direct way of measuring the nucleon momentum distribution inside the deuteron. The coincidence cross section is closely related to the momentum density. The latter having a transparent interpretation as in terms of S- and D-wave functions: $\rho(p) = |u(p)|^2 + |w(p)|^2$.

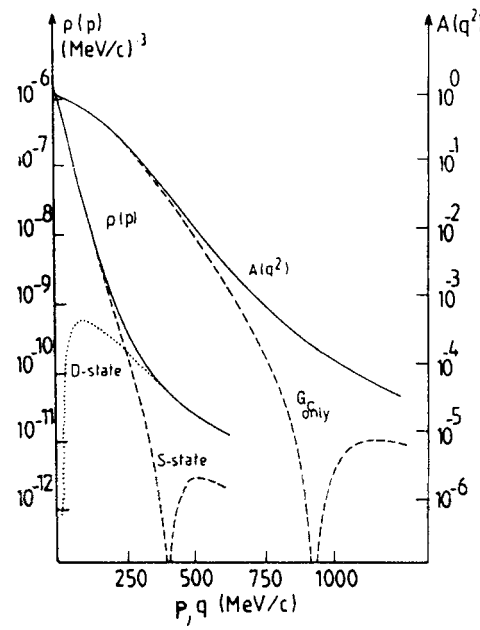

Fig. 3. Deuteron momentum density $\rho(p)$ and structure function $A(q^2)$ calculated from the RSC potential model.

Figure 3 shows the S/D-composition of $\rho(p)$ and $A(q^2)$ as a function of momentum (in the density p is the initial proton momentum, while for the structure function q is the four-momentum transfer). It demonstrates that the ^{2}H(e, e'p) reaction allows the study of the high relative momentum components of the deuteron wave functions using smaller momentum transfers than needed for elastic electron scattering experiments exploring identical momentum values.

In the quasi-free scattering process energy $\omega = e - e'$ and momentum $\vec{q} = \vec{e} - \vec{e}'$ are transferred from the incident electron to the target proton. This proton, with initial momentum $\vec{p}$, is subsequently ejected with a final momentum $\vec{p}'$, (total energy $E'_{\rm p}$). The residual neutron recoils with a momentum $\vec{n}'$ (total energy $E'_{\rm n}$). In this approximation one defines the 'missing momentum' $\vec{p}_{\rm m} = \vec{p} = -\vec{n}' = \vec{p}' - \vec{q}$ and the 'missing energy' as $E_{\rm m} = \omega - E'_{\rm p} - E'_{\rm n} + M_{\rm p} + M_{\rm n}$.

The six-fold differential cross section can be written as

$$\frac{{\rm d}^6\sigma}{{\rm d}\Omega^{\rm lab}_{e'}{\rm d}e'^{\rm lab}{\rm d}\Omega^{\rm cm}_{\rm np}{\rm d}E'_{\rm p}} = \frac{\alpha}{6\pi^2}\frac{e'^{\rm lab}}{e^{\rm lab}q^4_\mu}[\rho_{\rm L}f_{\rm L} + \rho_{\rm T}f_{\rm T} + \rho_{\rm LT}f_{\rm LT}\cos\Phi + \rho_{\rm TT}f_{\rm TT}\cos 2\Phi]. \tag{11}$$

In the one-photon exchange plane wave impulse approximation (PWIA), the cross section reduces to

$$\frac{{\rm d}^6\sigma}{{\rm d}\Omega_{e'}{\rm d}e'{\rm d}\Omega_{p'}{\rm d}E'_{\rm p}} = p'E'_{\rm p}\sigma_{\rm ep}S(E_{\rm m}, p_{\rm m}), \tag{12}$$

where $\sigma_{\rm ep}$ is the off-shell electron-proton scattering cross section and $S(E_{\rm m}, p_{\rm m})$ is the so-called spectral function. The spectral function is closely related to the momentum density, $S(E_{\rm m}, p_{\rm m}) = \rho(p_{\rm m})\delta(E_{\rm m} + E_{\rm B})$, where $E_{\rm B} = -2.225$ MeV is the binding energy of deuteron.

The cross sections obtained for the ^{2}H(e,e'p) reaction are well described by the Paris NN potential provided that final-state interaction and MEC effects are fully taken into account. This should allow a reliable extraction of the momentum distribution from the unpolarized data. Therefore, spin-dependent quasi-free electron scattering would be a meaningful next step in understanding the deuterium nucleus. Coincidence $^2\vec{\rm H}$(e,e'p) experiments will be extremely valuable, as they will provide an unambiguous measurement of the D/S ratio as a function of internal momentum.

2.3 Spin-dependent ^{2}H(e,e'p) quasi-elastic scattering

Including target polarization, the differential cross section $= S(h, P^{\rm d}_1, P^{\rm d}_2)$ can be written in the following form

$$\frac{{\rm d}^6\sigma}{{\rm d}\Omega^{\rm lab}_{e'}{\rm d}e'^{\rm lab}{\rm d}\Omega^{\rm cm}_{\rm np}{\rm d}E'_{\rm p}} = \frac{\alpha}{6\pi^2}\frac{e'^{\rm lab}}{e^{\rm lab}q^4_\mu}\Bigg\{\rho_{\rm L}f_{\rm L} + \rho_{\rm T}f_{\rm T} + \rho_{\rm LT}f_{\rm LT}\cos\Phi$$

$$+ \rho_{\rm TT}f_{\rm TT}\cos(2\Phi) + P^{\rm d}_1\Bigg[(\rho_{\rm L}f^{11}_{\rm L} + \rho_{\rm T}f^{11}_{\rm T})d^1_{10}(\Theta_{\rm d})\sin(\Phi - \Phi_{\rm d}) +$$

$$+ \sum_{M=-1}^{1} (\rho_{\rm LT} f_{\rm LT}^{1M} \sin\xi_M + \rho_{\rm TT} f_{\rm TT}^{1M} \sin\Psi_M) {\rm d}^1_{M0}(\Theta_{\rm d}) \Bigg]$$

$$+ P_2^{\rm d} \Bigg[\sum_{M=0}^{2} (\rho_{\rm L} f_{\rm L}^{2M} + \rho_{\rm T} f_{\rm T}^{2M}) d^2_{M0}(\Theta_{\rm d}) \cos(M(\Phi - \Phi_{\rm d}))$$

$$+ \sum_{M=-2}^{2} (\rho_{\rm LT} f_{\rm LT}^{2M} \cos\xi_M + \rho_{\rm TT} f_{\rm TT}^{2M} \cos\Psi_M) d^2_{M0}(\Theta_{\rm d}) \Bigg] \Bigg\},$$

where

$$\xi_M = M(\Phi - \Phi_{\rm d}) + \Phi \quad \text{and} \quad \Psi_M = M(\Phi - \Phi_{\rm d}) + 2\Phi . \tag{13}$$

Θ and Φ are the angles of the final np relative momentum with respect to the photon direction. $\Theta_{\rm d}$ and $\Phi_{\rm d}$ are the polarization orientation in the same coordinate system (see Fig. 4). $P_1^{\rm d} = P_{10}^{\rm d} = \sqrt{\frac{3}{2}}(n_+ - n_-)$, $P_2^{\rm d} = P_{20}^{\rm d} = \frac{1}{\sqrt{2}}(1 - 3n_0)$ are the usual vector and tensor polarizations of the deuteron.

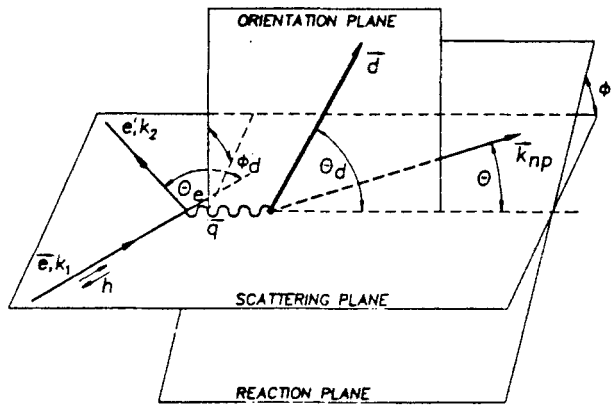

Fig. 4. Kinematics for the polarized $^2\vec{H}(e,e'{\rm p}){\rm n}$ reaction.

The ρ's are the spherical components of the virtual-photon density matrix. In a coordinate system with the z-axis parallel to $\vec{q}$, y-axis parallel to $\vec{e} \times \vec{e}'$, they can be written as

$$\rho_{\rm L} = q_\mu^2 \frac{\xi^2}{2\eta}, \quad \rho_{\rm T} = \frac{1}{2} q_\mu^2 \left(1 + \frac{\xi}{2\eta}\right),$$

$$\rho_{\rm LT} = q_\mu^2 \frac{\xi}{\eta} \sqrt{(\xi + \eta)/8}, \quad \rho_{\rm TT} = -q_\mu^2 \frac{\xi}{4\eta},$$

$$\rho'_{\rm LT} = \frac{1}{2} q_\mu^2 \frac{\xi}{\sqrt{2\eta}}, \quad \rho'_{\rm T} = \frac{1}{2} q_\mu^2 \sqrt{(\xi + \eta)/\eta}, \tag{14}$$

with $\xi = q_\mu^2/\vec{q}^{\,2}$ and $\eta = \tan^2 \frac{1}{2}\theta_{\rm e}$. Note that center of mass instead of the laboratory variables are used.

The f functions are defined as the deuteron structure functions and their components for an oriented target nucleus. They contain the relevant nuclear-structure information. Here, we only use the results derived by Arenhövel [6]. Experiment 91-12 will measure the asymmetry in scattering unpolarized electrons from tensor polarized deuterium.

$$A_{\mathrm{d}}^{\mathrm{T}} = \frac{1}{2P_2^{\mathrm{d}}S(0,0,0)}\Big[S(0,P_1^{\mathrm{d}},P_2^{\mathrm{d}}) + S(0,-P_1^{\mathrm{d}},P_2^{\mathrm{d}}) - 2S(0,0,0)\Big] =$$

$$= \frac{c}{S_0}\Bigg[\sum_{M=0}^{2}(\rho_{\mathrm{L}}f_{\mathrm{L}}^{2M} + \rho_{\mathrm{T}}f_{\mathrm{T}}^{2M})d_{M0}^2(\Theta_{\mathrm{d}})\cos(M(\Phi-\Phi_{\mathrm{d}}))$$

$$+ \sum_{M=-2}^{2}(\rho_{\mathrm{LT}}f_{\mathrm{LT}}^{2M}\cos\xi_M + \rho_{\mathrm{TT}}f_{\mathrm{TT}}^{2M}\cos\Psi_M)d_{M0}^2(\Theta_{\mathrm{d}})\Bigg]. \qquad (15)$$

3 Overview of the experiment

The goal of the experiment was to measure the spin-dependent cross-section for both ^{2}H(ee) elastic and ^{2}H(e, e'p) quasi-elastic scattering over a large kinematic range. The electrons are incident with momentum $k = (E, \vec{k})$ and scatter to final momentum $k' = (E', \vec{k}')$. The general expression for the cross section for polarized deuteron electrodisintegration has the following form:

$$\sigma = \sigma_0\Bigg[-\frac{\sqrt{3}}{2}P_z\sin\theta_{\mathrm{d}}\sin\phi_{\mathrm{d}}T_{11} + \frac{\sqrt{2}}{2}P_{zz}\Bigg(\frac{3\cos^2\theta_{\mathrm{d}}-1}{2}T_{20}$$

$$+ \sqrt{\frac{3}{8}}\sin 2\theta_{\mathrm{d}}\cos\phi_{\mathrm{d}}T_{21} + \sqrt{\frac{3}{8}}\sin^2\theta_{\mathrm{d}}\cos 2\phi_{\mathrm{d}}T_{22}\Bigg)\Bigg]. \qquad (16)$$

Here, σ_0 is the unpolarized cross section, P_z and P_{zz} are the degree of vector and tensor polarization defined as $P_z = n_+ - n_-$ and $P_{zz} = 1 - 3n_0$, where n_+, n_0, and n_- are the populations of the deuterium substates with the various nuclear spin projections on the direction of the magnetic holding field. The polarization direction of the deuteron is defined by the angles θ_{d} and ϕ_{d} in the frame where the z-axis is along the direction of the virtual photon and z-x is the reaction plane. T_{ij} are the analyzing powers of the reaction and experiment 91-12 measured both T_{20} and T_{22} for elastic scattering and quasi-elastic proton knockout. These observables are a direct measure of the spin structure of the deuteron ground state and should vanish in the absence of D-wave contributions.

Figure 5 shows a schematic layout of the experiment. The apparatus was designed to detect the scattered electron in coincidence with a knock-out proton or deuteron. The scattered electrons were detected at angles in the range $25° < \theta_{\mathrm{e}} < 40°$ with a calorimeter consisting of a plastic trigger scintillator (5 cm), a layer of CsI (6 cm thickness or 3.24 radiation lengths), another plastic trigger scintillator (1 cm), and the remainder of the CsI (30 cm). In front of the CsI proportional chambers were

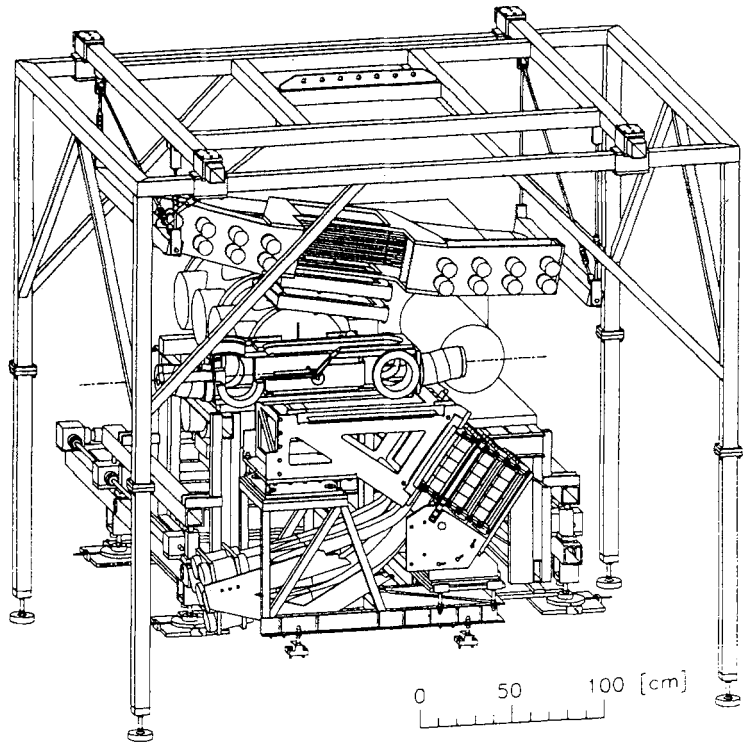

Fig. 5. A schematic layout of the experiment.

used to obtain tracking information on the θ_e and ϕ_e angles, and vertex position. The two MWPC's, each with an XY wire configuration, have a wire spacing of 2 mm and a separation of about 50 cm. Therefore, the intrinsic angular resolution amounts to about 10 mrad. The transferred momentum in experiment 91-12 amounts to $0.05 < q^2 < 0.25$ (GeV/c)^2.

A range telescope consisting of 16 scintillators was used for hadron detection at angles in the range $57° < \theta_p < 110°$. The first scintillator had a thickness of 2 mm to facilitate p/d separation. All other scintillators had a 10 mm thickness. This detector can detect protons (deuterons) in the range of 20–160 (18–300) MeV with an energy resolution of about 3 % (FWHM). The first scintillator from the range telescope was located at a 63 cm distance from the target center which results in a 300 msr solid angle. MWPC's, two chambers with each an UYX configuration and a 6 mm wire-spacing for the readout, were used in front of the hadron detectors. These MWPC's give redundancy to the experiment, as for a coincidence event the vertex position is already determined by the electron detector.

The experiment was performed using an unpolarized electron beam stored in the AmPS ring (see Fig. 6). This ring is an electron pulse-stretcher with a circumference of 212 m. AmPS is fed by a medium-energy electron accelerator (MEA) which can accelerate a beam of electrons up to energies of 700 MeV. Long beam lifetimes

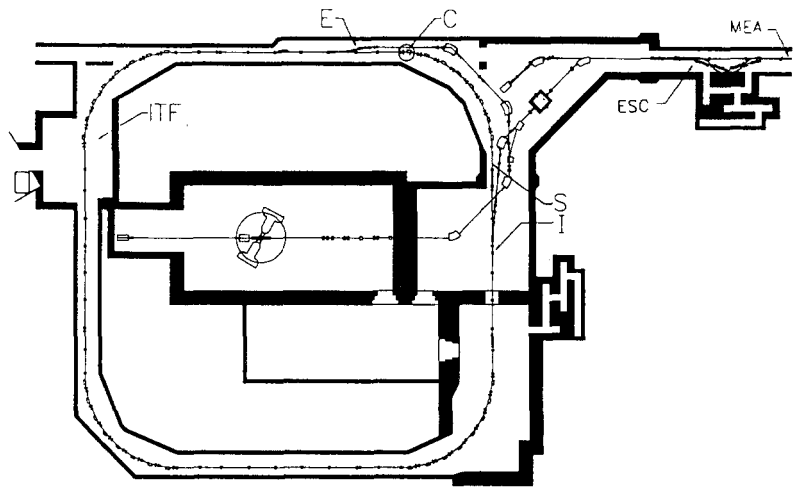

Fig. 6. A schematic layout of the AmPS Storage Ring. The stored beam is injected in Section I and can be extracted in Section E. Section A contains the apparatus for experiment 91-12. Beam scrapers are installed in Section S. Section C contains the 476 MHz cavity.

are obtained by compensating the loss in lifetime due to synchrotron radiation by a 476 MHz cavity in AmPS. In this way, a 100 % duty-cycle electron beam with energy of 565 MeV and current up to 120 mA (stacking) could be scattered from tensor polarized deuterons, delivered by an atomic beam source (ABS). Using a window-less storage-cell target in the AmPS ring resulted in a luminosity for experiment 91-12 in excess of 10^{31} $e^- \cdot$atoms $cm^{-2}s^{-1}$. The storage cell was located in the Internal Target Facility (ITF) at NIKHEF where the beam had minimum β-function values. The target polarization was reversed every 10 sec independent of the status of the beam. The luminosity was monitored by measuring the target thickness and the circulating current separately. In addition, measurement of spin dependent elastic scattering from polarized ^{2}H was carried out simultaneous to the quasi-elastic data taking.

At regular intervals during the 91-12 experiment, molecular hydrogen gas was flowed in the target so that ^{1}H(e,e'p) elastic measurements were carried out. These elastic measurements served to calibrate the time-of-flight system, monitored the stability of the electronics, allowed a determination of the kinematic resolutions, and provided information on the background rate. Further, measurements with an empty target were performed periodically to obtain information on background events.

When used with a large acceptance detector, this beam-target configuration had several advantages over conventional polarized targets. The target contained only ^{2}H atoms which were constantly replenished and the beam did not have to pass through any foils to reach the target. There was no radiation damage to the target and the magnetic holding field was 30 mT.

4 Polarized deuterium internal gas target

The polarized ^{2}H internal gas target consisted of a source of atoms directed into a thin-walled target cell. A differential vacuum pumping system interfaced the target cell to the storage ring vacuum. Figure 7 shows the experimental setup used to produce the polarized deuterium internal target.

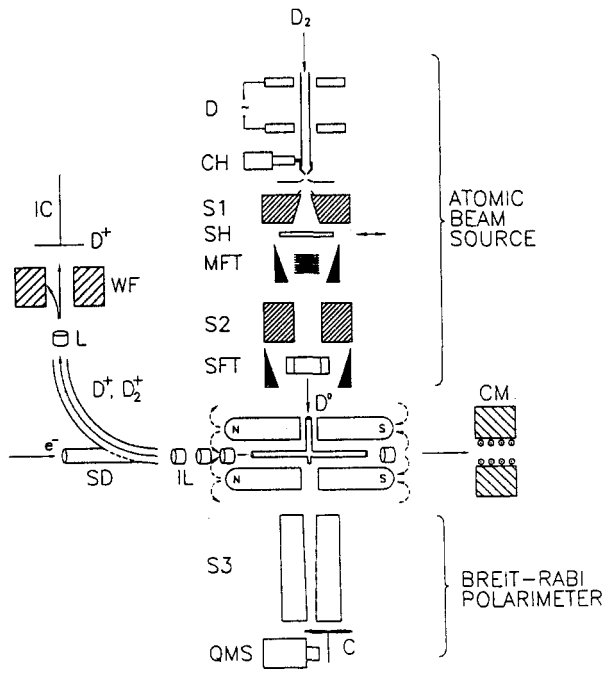

Fig. 7. Schematic outline of the atomic beam source (ABS), Breit-Rabi polarimeter (BRP), internal target, and ion extraction system. All components, except the target holding field magnets, are inside the vacuum system. D — RF dissociator; $S1$, $S2$, $S3$ — sextupole magnets; MFT, SFT — medium and strong field transition units; S — shutter; C — chopper; QMS — quadrupole mass spectrometer; CM — correction magnet; IL — triplet of ion extraction lenses; SD — spherical deflector; L — lens; WF — Wien filter; IC — ion collector.

A deuterium atomic beam is produced in an atomic beam source, ABS, ([10]) consisting of an RF dissociator, a cooled nozzle, collimators, sextupole magnets and RF transition units. The atomic beam is fed into the T-shaped storage cell located inside AmPS. About a 10 % fraction of the deuterium beam is analyzed with a Breit-Rabi electron polarimeter to monitor the intensity and polarization of the injected atoms. It consisted of a permanent sextupole magnet, a chopper and a quadrupole mass analyzer. A magnetic guide field is applied over the target region using two electromagnets. Note that the atomic beam reaches the target cell and the polarimeter through holes drilled into these holding field magnets. Ions

are formed due to ionization of the target gas by the circulating electron beam. The polarization of the atoms in the storage cell was determined by extracting and analyzing these ions using a combination of lenses, a spherical deflector, a Wien filter and a Faraday cup. Next, the various components will be discussed in more detail.

4.1 Polarized ^{2}H source

The ABS is based on the well-known principle of Stern-Gerlach separation of an atomic deuterium beam. An intense atomic beam is produced by means of an RF-dissociator with cooled nozzle (typically $\approx$ 70 K) and a powerful differential pumping system with a skimmer and a collimator. The upper hyperfine states with $m_J = +\frac{1}{2}$ (J = electron spin) are focused by a first sextupole magnet. In order to populate the required spin substates, high frequency transitions are induced. The tensor polarization P_{zz} was rapidly changed between $+1$ to -2. The polarized atoms were focused into a feed tube using a second compressor sextupole magnet. A flux of up to 2×10^{16} deuterium atoms s^{-1} in two hyperfine states was obtained. The ABS employed for experiment 91-12 was based on an existing apparatus. Therefore, the discussion will be restricted to the modifications of the ABS needed to achieve the highest possible flux and to make it compatible with running on AmPS.

Among the different RF transition schemes which can deliver tensor polarized deuterium beams the scheme was selected with the maximum figure of merit, defined as the product between ABS intensity, f_{ABS}, and ΔP_{zz}^2. For tensor polarization only one medium field transition unit (MFT) and one strong field transition unit (SFT) [11] are needed. The MFT was used to remove the dilution by hyperfine state 1 through a $1 \leftrightarrow 4$ transition (positive gradient) in between the sextupoles. The SFT was used to produce the actual tensor polarizations by flipping P_{zz} from -2 to $+1$ with the σ-transitions $3 \leftrightarrow 5$ and $2 \leftrightarrow 6$. For this scheme the target's magnetic holding field has to be strong compared to the critical field of deuterium. Note that for both tensor polarization states used in experiment 91-12 the corresponding vector polarization is equal to zero. The efficiency of the MFT and SFT units were monitored using the Breit-Rabi polarimeter while the efficiency of the MFT could also be determined by analyzing the extracted ions. The performance of the polarization scheme will be discussed in Section 5.

4.2 Polarized ^{2}H target

A schematic layout of the target chamber is shown in Fig. 8. The target chamber is made of stainless steel S.St. 304L, where in the center of the target cell a feed tube, aligned to fully accept the polarized gas from the ABS, is mounted together with an exit port for sampling the target gas with a Breit-Rabi polarimeter. In addition, a set of lenses and a spherical deflector are mounted for ion extraction polarimetry. The entire target chamber is installed on the ABS frame; while at each end of the target chamber, bellows are used to couple the target chamber to the ring. In between the ABS and target chamber a fast valve is employed. In order

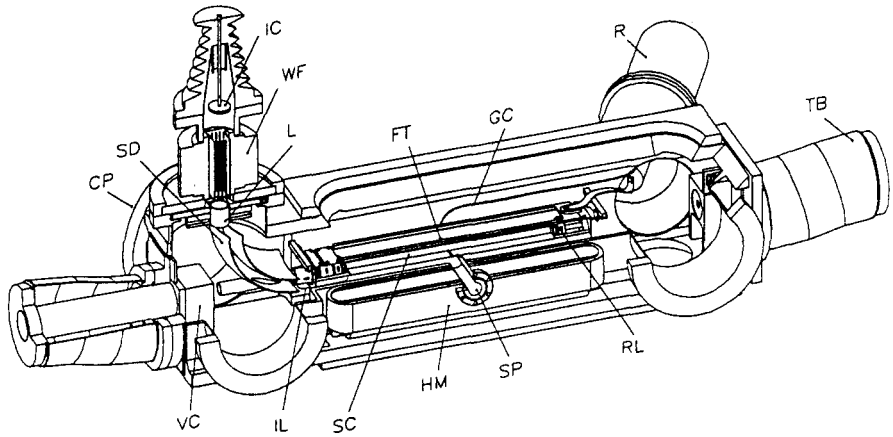

Fig. 8. A schematic layout of the target chamber. SC: storage cell; FT: feed tube; SP: sample port; HM: holding field magnet; RF: repeller lens; R: refrigerator; TB: tandem bellows; GC: gas-inlet capillary; IL: triplet of ion extraction lenses; SD: spherical deflector; L: lens; WF: Wien filter; IC: ion collector; VC: vacuum conductance limiter; CP: cryo pump.

to detect the low-energy recoiling particles, windows of S.St. foils with thickness of 0.1 mm were used.

For tensor polarized deuterium target, a strong magnetic holding field is preferred in order to get high polarization. This requires the field to be 30 mT or above, about a factor of 2–3 higher than the critical field (117 Gauss) of atomic deuterium. Such a strong field has to be uniform over the entire cell region, and its direction variable in the scattering plane in order to allow measurement of the observables T_{ij}.

The principal function of a storage cell is to increase the luminosity of the experiment without affecting the quality of the stored beam. The storage cell consisted of a straight tube through which the stored electron beam passed, an entrance tube for feeding the polarized gas into the storage cell and an exit port to sample the intensity and polarization of the injected target gas. For application in electron rings a straight tube is favored for the shape of the storage cell in order to prevent trapping of electromagnetic wake fields due to single- and multi-bunch effects of the electron beam. In general, the magnitude of these RF effects scale with the bunch charge squared ($\sim q_b^2$) and vary strongly depending on the specific machine (and tune of the machine).

The cell was cooled to 80 K using a cryogenic system based on a closed-cycle He refrigerator, which resulted in a sturdy system with reliable operation. The layout of the storage cell is shown in Fig. 9.

The parameters that govern the luminosity can be approximately written as

$$Lum \sim I_e f_{\mathrm{ABS}} \frac{L^2}{D^3} \sqrt{\frac{M}{T}}\,, \tag{17}$$

where I_e is the electron beam current, f_{ABS} the injected intensity of deuterium

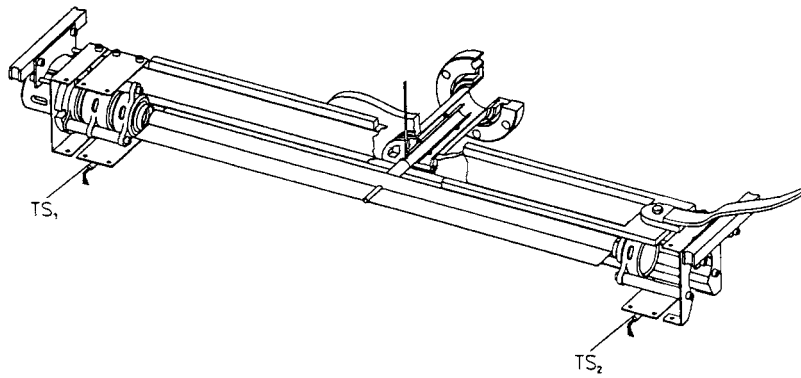

Fig. 9. A schematic layout of the target cell. TS_1 and TS_2 indicate temperature sensors.

atoms, L the length of the target cell, D the diameter, M the target mass and T the temperature. From this expression it is clear that one will try to minimize the diameter, increase the length and lower the temperature of the cell.

The target cell walls must be coated with special materials which inhibit depolarization and recombination. The most detailed study [12] of surface coatings was performed at UW-Madison. Here, an intense deuteron beam (50 keV, 0.25 mA) was sent through a cell in order to probe the electron polarization of hydrogen gas in a weak guiding field. Due to the coupling of the proton and electron spin, the nuclear polarization was tested in this experiment. Measurements were performed with metal cells, coated with aluminium oxide, Teflon, Viton and other materials, in a temperature range from 30 to 300 K. Cells with different geometry were used, which correspond to average numbers of wall collisions of 40, 150 and 380. The results obtained with these tests indicated that aluminum cells coated with Teflon represented the optimal storage cell configuration. Best performance was obtained for storage cells operated at 80 K. Additional measurements showed that in a strong target field environment the performance even improves [13].

In summary, the cell for experiment 91-12 had a 15 mm diameter and a length of 400 mm. The feed tube had a diameter of 12 mm and a length of 130 mm, while the hole towards the Breit-Rabi polarimeter had a 4 mm diameter. The conductance of the cell is given by the sum of conductances and is dominated by the feed tube to the ABS. A flux of 10^{16} atoms s^{-1} resulted in a central density of $\rho_{\text{center}} = 10^{12}$ atoms cm^{-3}. The target thickness amounted to $t = 2 \times 10^{13}$ atoms cm^{-2} and with a beam current of 120 mA this resulted in a luminosity in excess of 10^{31} $e^- \cdot$atoms $cm^{-2}s^{-1}$.

4.3 Deuterium polarimetry

In spin physics experiments the target polarization needs to be continually monitored during data taking since there are various possible target depolarization mechanisms. The polarization of the injected atoms will be less than 100 % due to inefficiencies of the MFT and SFT units. The efficiency of the MFT was slightly

below the maximum due to the influence of the fringe fields of the first sextupole magnet. Thus the injected atoms will have a contribution of hyperfine state 1 and this will result in a dilution of the tensor polarization. Furthermore, the rejection efficiency of the compressor sextupole is limited. This will result in a contribution of state 4 to the injected atoms, again diluting the tensor polarization. The degree of dissociation is limited to typically $\alpha \approx 0.6$ and given the finite magnification factor of the sextupole, ≈ 12, there will be molecules injected into the storage cell. These are unpolarized and will dilute the polarization. Furthermore, the storage cell will receive a contribution from unpolarized background gas, mainly D_2, from the ABS and the target chamber. The atoms are injected into the storage cell through a hole drilled into the holding field magnet. Components of the magnetic field will have zero crossings and it is important to measure polarization losses, if any, during injection.

In the storage cell there are additional mechanisms to affect the target polarization. The strength of the magnetic holding field determines the magnitude of the target polarizations since the tensor polarizations of the individual hyperfine states are field dependent. There is a magnetic field associated with the stored electron beam, due to the small current densities only on the order of a few Gauss. Little effect is expected from the direct interaction of this field with the magnetic moment of the atom. However, resonant depolarization can occur when an atomic transition frequency is an integral multiple of the frequency of the beam pulses. Given the 476 MHz for experiment 91-12, the first direct nuclear spin-flip resonance will occur at extremely high magnetic fields. However, the first electron spin-flip resonance occurs already near the distribution of our magnetic guide field, and consequently polarimetry is invaluable. The electron beam will also ionize the target atoms and molecules. Ion trapping will occur due to the electric and magnetic fields of the electron beam and will proceed until the density of the trapped ions becomes equal to the density of electrons in the beam. Finally, the polarized atoms interact with the walls of the storage cell and this can lead to depolarization due to spin-flip transitions and recombination. Studies [12] have shown that the P_{zz} of the atoms is quite robust and that polarization losses can be described by the time the atom spends on the surface of the cell wall. Significant polarization losses were only observed for $T_{\text{cell}} < 100$ K and can be attributed mainly to recombination. It has been shown [12] that after recombination the molecules have $P_{zz} \approx 0$. Therefore, it is crucial that the polarimetry is not restricted to the measurement of the polarization of the atoms. A proper assessment of the target polarization requires a measurement of the atomic and molecular fractions in the storage cell. Furthermore, it is not obvious that measurement of electronic polarization is sufficient for a determination of the nuclear polarization in a strong holding field environment.

4.3.1 Breit-Rabi electron polarimeter

The intensity and atomic polarization of the injected atoms was determined with a dedicated polarimeter. The basic idea of the Breit-Rabi polarimeter is to extract a small fraction of the injected gas ($\approx 10\%$) and to analyzed it with an atomic

beam detector. The Breit-Rabi Polarimeter consisted of a 44 cm long permanent sextupole magnet, with an entrance (exit) diameter of 6 (3) mm and a pole-tip field strength of 0.6 T, and a quadrupole mass analyzer. A chopper was used for background suppression.

The polarimeter was indispensable for proper tuning of the RF transition units. The working points of these units were affected by the stray fields from the target holding field and tuning was needed for each direction of the target spin. The $1 \leftrightarrow 4$, $2 \leftrightarrow 6$ and $3 \leftrightarrow 5$ transitions employed in experiment 91-12 all involve a collective electronic and nuclear spin flip. Therefore, a measurement of the electronic polarization could be used to determine the efficiencies of the MFT and SFT. The polarimeter was used to establish that no loss of polarization was induced by the stored electron beam or due to passage of the atoms through the holes in the target holding field magnets. Furthermore, the polarimeter allowed the optimization of the intensity of atoms injected into the storage cell as function of nozzle temperature, D_2-flow into the dissociator, discharge level, and sextupole field strengths. The performance of the Breit-Rabi polarimeter will be discussed in Section 5.

4.3.2 Analysis of ions extracted from the storage cell

The layout of the ion-extraction system is shown schematically in Fig. 10. The circulating electron beam ionizes the target gas in the storage cell. At the electron energy of 565 MeV the ionization cross section for atoms (molecules) amounts to 1.3 (2.6) $\times 10^{-19}$ cm^2. In order to prevent the ions from reaching the walls of the storage cell, where they would neutralize, depolarize and/or recombine, they were confined through the use of a ($\approx$ 300 G) longitudinal magnetic holding field and/or the space charge of the stored electron beam. The ions were reflected on one side of the cell using an electrostatic repeller lens. On the other end of the cell the ions were extracted using a triplet of electrostatic lenses. The extracted ions were then deflected out of AmPS using a spherical capacitor. The deflector focused the ions onto a Wien filter ($\vec{E} \times \vec{B}$ velocity selector) which allowed to separate atoms from molecules. The determination of the molecular fraction, which is known to be largely unpolarized, is important in order to precisely establish the target polarization.

A measurement of the atomic and molecular fractions is equivalent to a polarization measurement under the assumptions that the polarization of the injected atoms is known and that recombination is the sole source of depolarization in the storage cell. This was established in a separate experiment, where the extracted atoms were accelerated into an appropriate analyzer. The reaction ^{3}H(d,n)^{4}He was employed in order to measure P_{zz} directly. This reaction has the advantage of having a high cross section ($\sigma_{\text{total}} = 5$ barns at $T_{\text{d}} = 110$ keV) as well as good sensitivity in the neutron anisotropy to the deuteron tensor polarization. Several aspects of ion extraction from a storage cell target were tested and the most important finding will be reported in Ref. 14.

In summary, polarimetry by analyzing the extracted ions has the advantage that a) the polarization of the target is determined with the same weighting over gas density as in the actual experiment (in contrast to sampling polarimeters); b) the

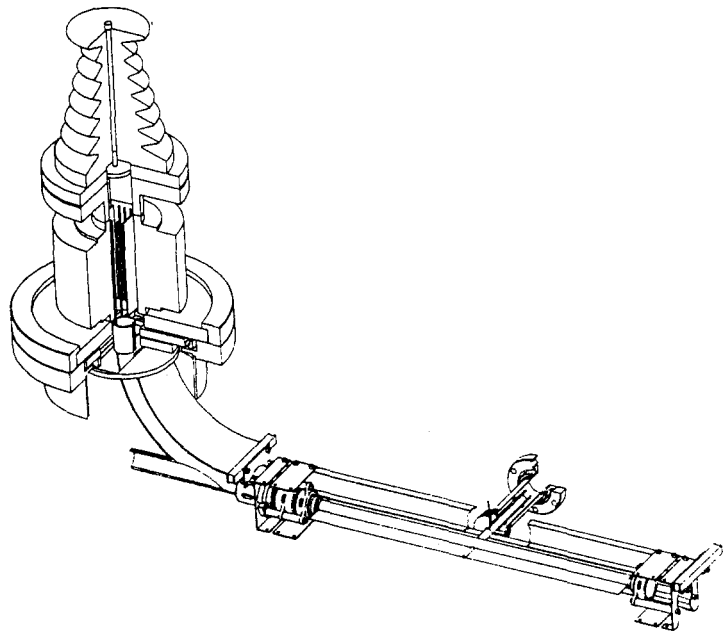

Fig. 10. Polarized atoms are ionized in the target cell by the circulating electron beam passing through the storage cell. The ions are extracted using a set of cylindrical lenses and deflected out of the electron beam path using a spherical capacitor. The ions pass through a Wien filter and are subsequently accelerated into the Faraday cup.

relevant nuclear polarization is measured (instead of deducing this from i.e. atomic polarization; c) the atomic and molecular fractions are measured.

5 Performance

The performance of the ABS was measured with different devices. In the first place, a cross-beam QMS was mounted at the location of the target cell to measure the atomic beam density. By turning on and off the sextupole magnets one can determine the amplification factor α of the sextupoles. Figure 11 shows α as function of the nozzle temperature for deuterium. The square data point shows the value obtained with the same ABS equipped with a half tapered first magnet (Singy et al.), instead of a continuously tapered, as is the case in the ABS used for the 91-12 experiment. The half-tapered magnet delivers more atomic beam intensity. The amplification factor was also measured as function of the sextupole magnet currents. It was found that the first sextupole attains a saturation value, which indicates that the magnet is strong enough, even at a nozzle temperature $T_{\mathrm{nozzle}} = 70\,\mathrm{K}$. On the contrary, the second magnet does not attain such a saturation value, even at the design nozzle temperature of 35 K. A stronger compressor magnet could provide a noticeable increase of the atomic beam intensity. With this setup, the rejection

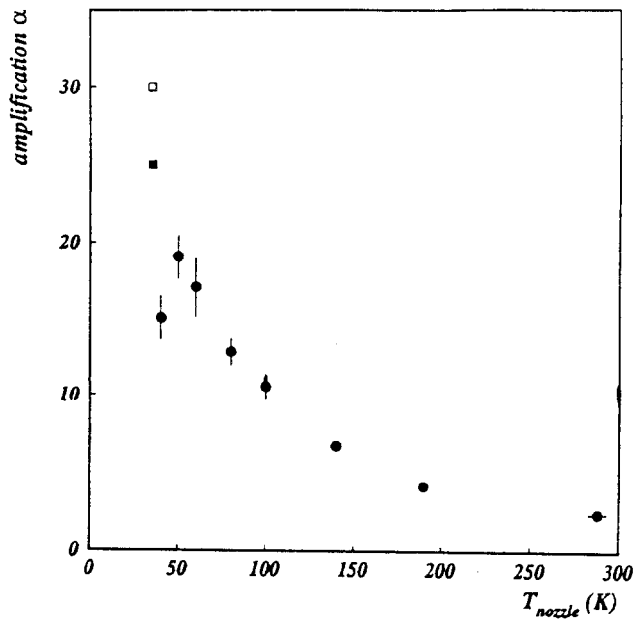

Fig. 11. Amplification factor of the sextupoles for a deuterium beam measured with a QMS as function of the nozzle temperature. The crosses show the result of a raytrace calculation. The square is the value measured by Singy et al. [10] with the same ABS equipped with a half tapered first magnet, instead of a continuously tapered, as is the case in the ABS used for the 91-12 experiment.

efficiency by the second sextupole of the deuterium hyperfine state 4 induced by the MFT could also be extracted by turning on and off the MFT.

The performance of the RF-units measured with the Breit-Rabi polarimeter has been exhaustively described elsewhere [11]. In Fig. 12 the main result of these measurements are presented. The amount of atoms detected by the QMS located after the permanent sextupole is shown as function of the central magnetic field in the SFT and MFT units. A drop of one third with respect to the 3-hyperfine-states intensity indicates a 100 % efficiency of the transition. In Fig. 12 three subsequent scans over the static magnetic field of the MFT are shown. The first scan (solid curve) is carried out with the SFT turned off. The drop of the QMS response in the range $B \approx 1.1$ to 1.8 mT indicates that the MFT populates state 4, since, of the hyperfine states present just after the MFT, only state 4 is rejected by the second and third sextupoles. The next two scans are done with the SFT turned on and tuned to the 2-6 (dotted curve) or the 3-5 transition (dashed curve). This allows to determine which states (1, 2 or 3) have been transfered to state 4 by the MFT. For instance, the 2-6 and 3-5 SFT will produce an additional 1/3 drop of the QMS response with respect to the data with the SFT off, unless the MFT reduced the population of state 2 and 3, respectively. In this way, one can locate the 1-4, 2-4 and 3-4 transitions.

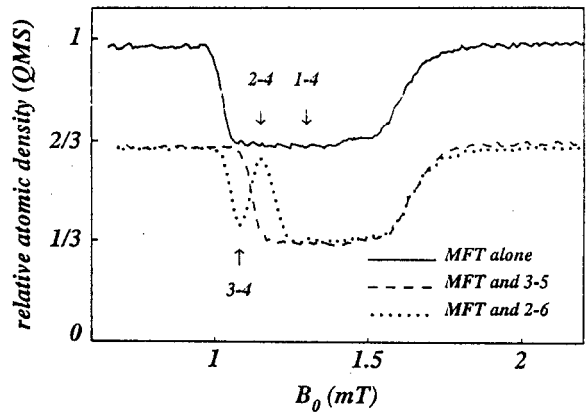

Fig. 12. Relative atomic beam density measured with the Breit-Rabi polarimeter as function of the central magnetic field of the SFT and MFT units. For the MFT three scans are carried out to identify the 1-4, 2-4 and 3-4 transitions (solid curve: SFT off, dotted curve: SFT tuned to 2-6, dashed curve: SFT tuned to 3-5).

The transition efficiencies in the internal target environment, characterized by strong fringe fields and gradients, are close to unity for the 2-6, 3-5 and 1-4 transitions. This result could be obtained at various values and orientations of the target holding field. These measurements also prove that the atoms do not lose their polarization when passing through the target holding field magnets, where the magnetic field changes sign. In addition, no depolarization of the direct atomic beam by the electron beam was observed at currents as high as 120 mA and energies ranging from 450 to 570 MeV.

Next, we discuss the results obtained from an analysis of ions extracted from the storage cell. Figure 13 shows a velocity spectrum measured in experiment 91-12. The velocity spectra reveal that there is a significant dilution of the target polarization by molecules. More than half of the molecules in the target cell actually arise not from recombination but from molecules originating in the atomic beam source and entering the target cell together with atoms through the cell entrance tube. This indicates that the improvement in the degree of dissociation not only would give higher ABS intensity but would also reduce the molecular dilution to the target polarization.

The net target polarization is the mean of the D^+ and D_2^+ polarizations, each weighted by the fractional contribution they make to the total number of the target atoms, and is expressed by,

$$P_{zz} = \frac{n_D P_{zz}(D^+)}{n_D + 2n_{D_2}} = \frac{i_{D^+} P_{zz}(D^+)}{i_{D^+} + i_{D_2^+}}, \tag{18}$$

where, n represents density and i ion current. The D_2^+ polarization is taken to be zero. $P_{zz}(D^+)$ has been measured separately by using a tritium polarimeter with

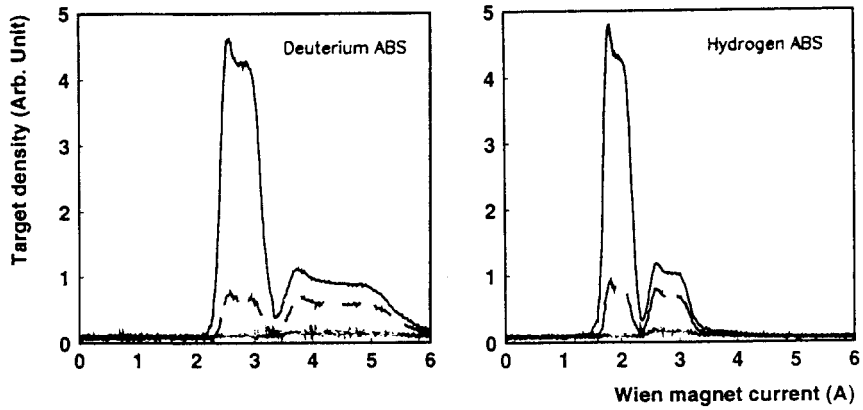

Fig. 13. Ion current transmitted through Wien velocity filter as a function of the Wien $\vec{B}$-field current. Lower velocity and higher velocity peaks are caused by D^+ and D_2^+ (left), or H^+ and H_2^+ (right), respectively. The solid curves are full ABS intensities; while the dashes correspond to zero sextupole currents. The dotted lines show the empty cell with the ABS beam shuttered. Note that the ion current is normalized by the electron beam current.

our test chamber where the ions, ionized by 1 kV e-gun beam through the cell, are extracted in the same way, but without a spherical deflector, and then accelerated to 50 keV energy to bombard a tritiated Ti target. The measured value is about 70% of the maximum and is consistent with the deficit due to the RF transition inefficiencies, the second sextupole rejection ratio, and finite target holding B-field. The resulting net polarization is around 50%. A future plan of measurering P_{zz} with a tritium target in the ring vacuum to measure the D^+ ion polarization on-line, is under consideration.

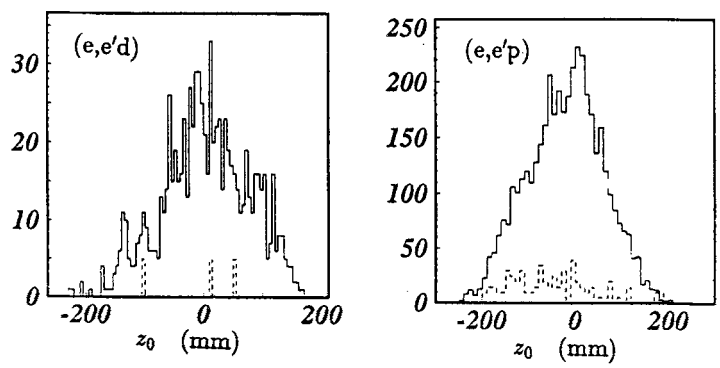

Fig. 14. Reconstructed vertex position along the beam axis from wire chamber raytracing for the reactions ^{2}H(e,e'd) and ^{2}H(e,e'p) for measurements with the ABS (solid curve) and empty storage cell (dashed curve).

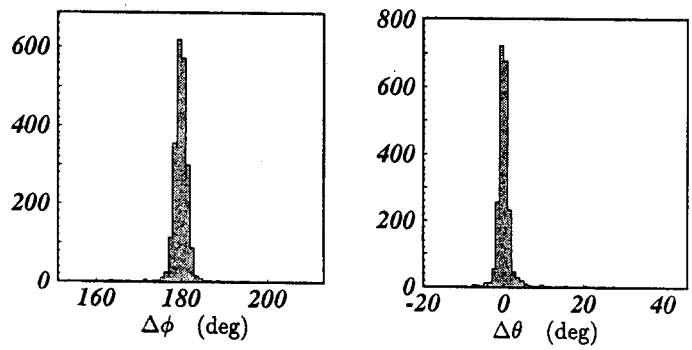

Fig. 15. Coplanarity distribution $\phi_e - \phi_p$ of ^{1}H(e,e'p) elastic scattering events. The figure also shows the distribution $\theta_p - \theta_q$, where the latter is determined from the electron kinematics.

Finally, we will discuss the vertex reconstruction and background study. One of the principal advantages of the polarized internal target technique is the possibility to perform scattering experiments using an isotopically and chemically pure target species. High purity (99.99%) polarized ^{2}H gas atoms are injected into the storage cell at the center. The gas flows out the open ends of the cell resulting in a density distribution that is approximately triangular and centered on the cell. Figure 14 shows the vertex distribution along the beam axis (z) from wire chamber ray-tracing of the ^{2}H(e,e'd) and ^{2}H(e,e'p) reaction for measurements with and without (shuttered) the ABS. The distributions are in good agreement with the expected shape and indicate that backgrounds are negligible for elastic scattering and small for quasi-free scattering. In addition, their effects can be determined precisely.

In order to make quantitative estimates of the background in the quasi-elastic scattering measurements, e.g. from either the walls of the cell or unpolarized background gas outside the cell, it was necessary to take data on scattering from hydrogen gas. Such measurements were also made with an empty cell, but the beam phase space properties could be different since they are determined from a complicated interplay of emittance growth effects due to scattering in the target and damping effects. Figure 15 shows the distribution of the correlated outgoing particle angles for ^{1}H(e, e'p). The coplanarity distribution is peaked at around $\phi_e + \phi_p = 180°$(FWHM $\approx 1°$) as expected for elastic scattering. Furthermore, the proton knockout angle is in good agreement with the angle expected from the electron kinematics.

6 Summary

A polarized ^{2}H internal gas target has been successfully used in a medium-energy storage ring with an electron beam to carry out spin-dependent scattering measurements. The unique advantages of internal targets such as purity, high polarization and the ability to manipulate the target spin have been demonstrated. A large acceptance detector has been used to simultaneously measure the scattering asymmetries in elastic and quasi-elastic scattering. The techniques developed in

this experiment for luminosity and polarization monitoring are of general importance for future experiments using polarized electron beams and polarized internal targets.

The target thickness of 2×10^{13} atoms/cm^2 was limited by the performance of the ABS and the quality of the stored electron beam. For future experimental configurations with medium-energy electron storage rings, the target thickness could be at least one order of magnitude thicker using a system of permanent sextupoles to increase the injected atomic deuterium flux and additional focusing of the electron beam to decrease the transverse dimensions of the target cell.

Experiment 91-12 has demonstrated that the use of polarized internal target and electron beam with a large acceptance detector allows the study of the spin dependent reaction over a large kinematic range with high statistical and systematic precision. Similar experiments planned with polarized electron beams should provide measurement of electromagnetic polarization asymmetries over a broad range of momentum transfer.

The author thanks the entire 91-12 collaboration and acknowledges interesting discussions with Henk Jan Bulten. The research is supported by the National Science Foundation under Contract No. PHY-9316221 and under a NATO Grant No. CRG920219.

References

[1] Gilman R. et al.: Phys. Rev. Lett. *65* (1990) 1733.

[2] FILTEX, CERN Proposal PSCC/P92, spokesman E. Steffens.

[3] HERMES, DESY Proposal, spokesmen R.G. Milner and K. Rith.

[4] IUCF experiment CE-25, spokesmen J.F.J. van den Brand and J. Sowinski.

[5] BLAST proposal at MIT-Bates, Spokesmen: J.F.J. van den Brand, R. Milner, R. Alarcon, R. Redwine and W. Hersman.

[6] Tomusiak E.L. and Arenhövel H.: Phys. Lett B *206* (1988) 187.

[7] Experiments: SMC at CERN, E143 and E155 at SLAC, HERMES at DESY.

[8] NIKHEF Experiment, spokesmen: C. de Jager, J.F.J. van den Brand and R. Holt (1994).
MIT-Bates Experiment, spokesmen: R. Alarcon and J.F.J. van den Brand (1991).

[9] The I. et al.: Phys. Rev. Lett. *67* (1991) 173.

[10] Singhy D. et al.: Nucl. Instrum. Meth. A *278* (1989) 349; B *47* (1990) 167; A *306* (1991) 36.

[11] Ferro-Luzzi M., Zhou Z.-L., Bulten H.J., and van den Brand J.F.J.: Submitted to Nucl. Instrum. Meth.

[12] Price J.S. and Haeberli W.: Nucl. Instrum. Meth. A *326* (1993) 416.

[13] Gaul H.G. and Haeberli W.: Private commun.

[14] Zhou Z.-L., Ferro-Luzzi M., Bulten H.J., and van den Brand J.F.J.: Submitted to Nucl. Instrum. Meth.